Torsvik, T. H., Steinberger, B., Gurnis, M., Gaina, C. (2010): Plate tectonics and net lithosphere rotation over the past 150 My. - Earth and Planetary Science Letters, 291, 1-4, 106-112

DOI: 10.1016/j.epsl.2009.12.055

Plate Tectonics and Net Lithosphere Rotation over the past 150 My

Trond H. Torsvik[1-3*], Bernhard Steinberger[4,1,2], Michael Gurnis[5], Carmen Gaina[2,1]

[1]Physics of Geological Processes & Geosciences, University of Oslo, Norway
[2]Centre for Geodynamics, NGU, Trondheim, Norway
[3]School of Geosciences, University of the Witwatersrand, Johannesburg, South Africa
[4]Helmholtz Centre Potsdam, German Research Centre for Geosciences, Potsdam, Germany
[5]Seismological Laboratory, California Institute of Technology, Pasadena, California, USA

***email:** t.h.torsvik@fys.uio.no

ABSTRACT

We have developed an improved model of global digital palaeo-plate boundaries and plate motion to describe the distribution and history of plates since the Late Jurassic. From this history we computed net lithospheric rotation (NR) through time confirming the so-called westward, but only for the past 30 Myrs. The NR has significantly smaller magnitudes (0.13°/My, past 5 My) than for some other plate models; it averages to 0.11 ± 0.03°/My for the past 50 My with a small but systematic increase toward the present. The westward drift, seen only for the past 30 My, is attributed to the increased dominance of a steadily growing and accelerating Pacific plate. NR shows peaks with time but only an Early Tertiary peak of 0.33°/My (when the Indian plate was undergoing the largest known acceleration/deceleration) can be interpreted with some confidence. We find a linear decreasing trend in net rotation over the past 150 My, but attribute this trend to increasing reconstruction uncertainties back in time, as subduction consumed more than half of the oceanic crust since the Jurassic. After removing a linear time-trend, we find a NR average of about 0.12°/My for the past 150 My.

*Keywords***:** Plate tectonics, global palaeo-plate boundaries, net lithosphere rotation, westward drift

1. Introduction

During the 20th century our description of the movement and deformation of the Earth's outer rigid layer evolved from the hypothesis of Continental Drift (Wegener 1915) into Sea-Floor Spreading (Hess 1962) and to the theory of Plate Tectonics (Wilson 1965, McKenzie & Parker 1967, Morgan 1968, Le Pichon 1968). Now a fourth shift is underway in which Plate Tectonics is being subsumed into a new Mantle Dynamics framework that requires plate motion reconstructions through time to include not only improved relative plate motions but also refined plate motions with respect to the mantle.

By combining relative and absolute plate motion frames from the Indo-Atlantic (Torsvik et al. 2008a; Steinberger & Torsvik 2008) and the Pacific (Steinberger & Gaina 2008) realms we have re-constructed first order palaeo-plate boundaries for the last 150 Ma. Based on the absolute plate motion frames (Table 1) and guided by numerous regional relative plate tectonic models (oceanic domains mostly summarized by Müller et al. 2008), we developed a global model of "tectonic plates polygons" for each 10 Myr interval since Late Jurassic (150 Ma). The plate polygons are closed polygons that outline a rigid block (tectonic plate) that has moved relative to neighboring rigid blocks for a finite amount of time as indicated by the type of the plate boundary between them (see Section 2). This global model can be used for many purposes in geodynamic modeling. Here we describe a single important example, namely the calculation of net lithosphere rotation (NR). If mantle convection is the principal driving mechanism for plate motions, NR should be zero unless individual lithospheric plates have different couplings to the underlying mantle flow. A proper reference frame with appropriate NR is important for discussions of poloidal/toroidal partitioning of plate motions (Lithgow-Bertelloni et al. 1993). Most plate models predict westward drift of the lithosphere with respect to the deep mantle, which has been ascribed to lateral viscosity variations (Ricard et al. 1991; O'Connell et al. 1991). Westward drift estimates vary considerably (1.5-9 cm/year) and are usually larger than those calculated from geodynamic models (Becker 2006). However, comparison of westward drift estimates with geodynamic models is problematic, since all geodynamic models are based on simplifying assumptions. Recently, seismic anisotropy has emerged as a further tool to estimate NR for recent times (Becker 2008; Kreemer 2009; Conrad & Behn, submitted Geochem. Geophys. Geosyst.). In Section 3 we explore NR, not only for present times but for the past 150 Ma.

2. Global Plate Polygons

Building global plate polygons through Earth history (Fig. 1; online supplement) requires knowledge of relative plate motions from both continental and oceanic areas. The uncertainty in constraining these motions increases for older times, due to the destruction (through subduction) or distortion (such as collision) of relative motion. For example, more than half of the oceanic crust created since the Jurassic has been consumed by subduction, therefore past plate boundary configuration has to be restored by making assumptions based on limited geological constraints (like the age of preserved ophiolites or slab-window related volcanism) and the rules of plate tectonics. World uncertainty – the fraction of the Earth's lithosphere which has been subducted since a given time, and for which plate motion at that time is therefore uncertain, reaches ~60% at around 140 Ma (Fig. 2b).

Starting with a simplified version of today's tectonic plate boundaries (mostly compiled from Bird 2003), plate polygons were constructed for each 10 Myrs with averaged Euler stage poles computed for 10 Myrs intervals. Polygons were originally constructed using GPlates (Boyden et al. 2010), partly using the continuously closing plate method (Gurnis et al. 2010) and subsequently modified and refined in Arc-GIS. The polygon boundaries and stage poles (online supplement) are based on a large number of sources but a large proportion originate from work by the Geodynamic Teams at NGU & PGP, Norway and the University of Sydney EarthByte Group, Australia (e.g. Alvey et al. 2008, Gaina et al. 1998, 2002, 2009, Gaina & Müller 2007; Heine et al. 2004; Müller et al. 2008; Torsvik et al. 2008a-b, 2009 *and references therein*).

In addition to the traditional plate polygon boundaries (ridge, trench and transform faults) we also include plate boundaries for rifts (divergent 'diffuse' boundaries) where we have been able to quantify the amount of rifting with some confidence. As an example, our 60 Ma reconstruction (Fig. 1b) treats Europe (plate number 301) as a distinct plate (i.e. not attached to Greenland, plate number 102, as it might be deduced from a pre-breakup configuration). At this time, although seafloor spreading was taking place in the Labrador Sea (between Greenland, together with SW Ellesmere and Devon Island, and North America) significant Late Cretaceous-Early Tertiary rifting also took place between East Greenland and NW Europe, and therefore a plate boundary between Greenland and Europe is incorporated to model this rifting. Similarly, at 100 Ma (Fig. 1c), Greenland is kept as a separate plate due to pre-drift rifting versus both North America and Europe. At this time Africa is also divided into three plates (plate numbers 701, 714-715) due to the minor intra-plate Cretaceous rifts that were active at this time. At 150 Ma (Fig. 1d), we combine most of South America and Africa as one plate ('Africa' 701) whilst Patagonia is treated as a separate plate (Torsvik et al. 2009). At this time we also combine East Antarctica (802), India (501), Madagascar (702) and Australia as one plate ('Australia' 801).

We stress that knowledge and data quality differs greatly for smaller areas, from excellent to poorly constrained, and many plate polygons can only be regarded as provisional. Some areas are heavily oversimplified (work in progress), but due to the relative small areas covered by some of these plates (e.g. within the Caribbean), revised boundaries will introduce only minor differences in the calculations of net lithosphere rotation (Section 3) or derivative geodynamic modeling.

3. Net Lithosphere Rotation

We computed net rotation of the entire lithosphere as:

$$\boldsymbol{\omega}_{net}=3/(8\,\pi\,r^4)\int \mathbf{v} \times \mathbf{r}\,dS = 3/(8\,\pi\,r^4)\Sigma_i \int(\boldsymbol{\omega}_i \times \mathbf{r}) \times \mathbf{r}\,dS_i\,,$$

where $\mathbf{v}$ is the velocity vector, $\boldsymbol{\omega}_i$ is the rotation rate vector of plate i, $\mathbf{r}$ is the position vector , $\int ...dS$ indicates integration over the entire sphere, Σ_i indicates summation over all plates, and $\int ...dS_i$ indicates integration over the area of plate i.

Figure 2b and Table 2 summarize NR calculations through geological time given our plate rotations and boundaries. We find 0.13°/My for the past 5 Ma, 0.14°/My for the past 10 Ma and 0.11 ± 0.03°/My for the past 50 My (N=5; mean and standard deviation of 10 Myr intervals). These are compatible with the NR estimates by Gordon & Jurdy (1986; 0.114°/Myr), Torsvik et al. (2008a; 0.165°/Myr for the past 5 Myr), and are only slightly higher than those obtained from numerical computations (~0.02-0.11°/My; orange ovals in Fig 2b; Becker 2006) and also compatible with NR estimates using seismic anisotropy: Becker (2008) finds that only NR up to ~ 0.2°/Myr is consistent with seismic anisotropy constrained by surface waves. By considering SKS splitting observations, Kreemer (2009) determines a best-fit NR of 0.2065°/Myr around a pole at 57.6°S, 63.2°E. Building upon both these works, Conrad & Behn (manuscript submitted *Geochem. Geophys. Geosyst.*) jointly constrain lithosphere NR and upper mantle viscosity and find that NR should not exceed 0.26°/Myr. Our NR vectors differ somewhat compared with previous studies; we obtain higher Euler latitudes (Fig. 4) and thus yielding a more well-defined westward velocity field for the past 30 million years (Fig. 3). The orientation of the axis of net rotation through time, computed here in a mantle reference frame (Fig. 4) also bears considerable resemblance to the no-torque reference frames of Čadek and Ricard (1992; their figs. 4 and 5).

Most plate models predict westward drift of varying magnitude; our model estimation has a westward drift at the equator of ~1.5 cm/year, but ~3 times lower than the 'young' hotspot model of Gripp & Gordon (2002; HS3 in Fig. 2b) and 3-6 times lower than those values estimated by Doglioni (2005) using alternative reference frames. The HS3 model is widely used and discussed in the recent geodynamic literature (e.g. Becker 2006; 2008; Funiciello et al. 2008; Husson et al. 2008) but differs from all other plate models in the sense that Africa and Eurasia (for example) are moving south-westward, i.e. opposite to our velocity fields (Fig. 1a; Table 1). No tracks on the African plate were used to construct the HS3 model. Morgan & Morgan (2007) have pointed out that the HS3 model yield a too high velocity for the Pacific plate (1.06°/Myr around a pole of 61.5°S, 90.3°E). Our model when averaged over the last 10 Myr gives a ~20% lower velocity for the Pacific (0.85°/Myr around a pole of 72.6°S, 116.3°E; online supplement Table S1). This is ~6% higher than the model of Morgan and Morgan (2007) with 0.80°/Myr around a pole of 59.3°S, 94.6°E, ~10% higher than the T22A model of Wang & Wang (2001) with 0.775°/Myr around a pole of 63.1°S, 103.9°E, and substantially higher than Pacific plate motions in a no-net rotation frame (e.g., Argus & Gordon, 1991; Kreemer & Holt, 2001).

Calculating NR through time we find a fluctuating pattern superimposed on a long term descending linear trend since 150 Ma (Fig. 2b, blue stippled line). However, the linear trend should be treated with caution because for older times the polygons containing oceanic areas became less well constrained. At 150 Ma the world uncertainty is ~60% using reconstructions that are based on a reasonably constrained Pangea undergoing breakup while surrounded by simplified oceanic areas in which little is known. Possible additional plate boundaries (like intra-oceanic subduction and adjacent back-arc spreading) are missing from this oceanic realm. Removing this linear trend leads to an average NR of around 0.12°/Myr for the past 150 Ma.

Another indication that this linear trend is an artifact while the average estimated NR is more robust comes from separate analyses of net rotation: for subducted plates only, for oceanic subducted plates only, and for corresponding complementary sets of plates (Fig. 5). We find that for recent times (last 20-30 Ma) net rotations for subducted plates only, and in particular for oceanic subducted plates only, are larger and around a similar axis as for all plates. Net rotations for the complementary sets (plates that are not subducted, and in particular non-oceanic plates) are smaller and around different axes – even close to opposite (angle nearly 180°) for the most recent time interval for plates that are not oceanic subducted. This is precisely what we expect from the dynamics of subduction: subducted slabs primarily pull the plates which they are attached to, but, through viscous coupling, also pull the overriding plates towards the trench. For times before about 40 Ma, on the other hand, net rotation for all subsets of plates tend to be around similar axes (small angles in Fig. 5b) which is contrary to expectations from dynamics and therefore again indicates shortcomings in the reference frame. In fact the slope of the dashed blue line in Fig. 2b (around 0.05 °/Myr/50 Myr) indicates that around 50 Ma the "artificial" net rotation becomes similar in magnitude to the net rotation of the plates that are not subducted or not oceanic subducted (i.e. the sets of plates complementary to 'oceanic and subducted'); this explains why around this time the transition from the "realistic case" with roughly opposite net rotation to the "unrealistic case" with similar net rotation of the not-subducted (or not oceanic subducted) plates occurs.

Some of the short-term fluctuations and changes could be real. For the last 50 My we notice a general increase from 0.08°/My (well within the range of geodynamic modeling results) to 0.13-0.14°/Myr, which can be attributed to a steadily growing and accelerating Pacific plate at the expense of a shrinking and decelerating Farallon plate (Fig. 2a) and subduction of the Izanagi plate. The Eocene burst of subduction initiation in the western Pacific (Gurnis et al. 2004) favored increased driving forces on the Pacific toward the west that may have contributed to the progressively increasing NR since 50 Ma. We conclude that the westward drift is real but only pronounced for the past 30 My and caused by the large and fast Pacific oceanic plate.

The magnitude of the velocity for a few selected plates is shown in Figure 2a. In addition to the purely oceanic Pacific and Farallon plates we also show the velocity field evolution for Africa (mostly continental and shown as a bar graph since it is our main reference plate) and the Indian plate where the ratio of continental vs. oceanic area has varied substantially through time (see Fig. 1a-d). During the Mid to Late Cretaceous separation of India and the Seychelles from Madagascar (Torsvik et al. 2000), the Indian plate accelerated to speeds of more than 15 cm/year (60-50 Ma) followed by a rapid decrease (50-40 Ma) to ~5 cm/year after collision with Eurasia. This is the largest known acceleration/deceleration and is clearly reflected in NR calculations that show a peak between 60-50 Ma (0.33^{o}/Ma). However, this peak is significantly smaller than present day values estimated from the HS3 model. In order to explore the significance of this peak we also tested two other Indo-Atlantic plate models (maintaining the same Pacific model), a fixed hotspot model and a different moving hot spot model (Fig. 2b). We notice that the 60-50 Ma peak is visible in all reference frames but somewhat subdued compared with our model. Any earlier fluctuations differ among the different reference frames; deviations from the linear trend generally do not exceed errors in net rotation inferred from that trend, and are hence not considered robust model features. For a consistent treatment, changing the reference frame in the Pacific and/or African hemisphere also implies changing plate boundaries accordingly. In our online supplement, we hence also include a program that, from a given plate boundary set (also supplied online) that is consistent with the Africa and Pacific rotations given in Table 1, computes boundaries consistent with different absolute rotations for these two plates, while relative rotations within the Pacific and African hemispheres remain the same.

4. Conclusions and future outlook

We have used an improved model of digital plate boundaries and absolute plate motions through time to compute net lithosphere rotation (NR). We draw the following conclusions:

1. NR with respect to the mantle has been ~0.13^{o}/My for the past 5 My and 0.11 ± 0.03^{o}/My for the past 50 My.
2. NR is approximately westward (~1.5 cm/yr), but only for the past 30 My (Figs. 3-4). It is currently dominated by Pacific plate motion.
3. NR has increased from ~0.08^{o}/My during the past 50 My (Fig. 2b). That we attribute to a steadily growing/accelerating Pacific plate.
4. NR magnitudes are three times lower than the HS3 model (Gripp & Gordon 2002) and we recommend that this model, which differs from all other published hotspot and mantle models, should be used with caution (at least in the Indo-Atlantic domain).
5. NR show a pronounced peak (0.33^{o}/My) between 60 and 50 Ma. We consider that this peak in NR was caused by the Indian plate accelerating to speeds of more than 15 cm/year followed by a rapid deceleration after India collided with Eurasia (5 cm/yr).

NR fluctuates and gradually increases back in time, and by removing a linear time-trend in the data (Fig. 2b), averages to ~0.12°/Myr for the past 150 Myr. However, the oceanic area reconstructions rely on few constraints and many assumptions for older time intervals; about 60% of the lithosphere have been subducted since 150 Ma and plate motions are uncertain for this fraction. To realistically reconstruct the proto-Pacific through time, information about the oceanic crust consumed by subduction is needed. Subducted material is imaged by tomographic models (e.g. van der Meer et al. 2010) and we envisage that the next generation of global plate reconstructions and plate boundaries will incorporate at least the first order estimate of the amount of subducted material based on tomography and iterative plate reconstructions.

Acknowledgements

We thank Giampiero Iaffaldano for stimulating one of us (THT) to gain interest in developing a revised model of global digital palaeo-plate boundaries, Kevin Burke, Yanick Ricard (Editor) and three anonymous referees for comments, and Statoil and the Norwegian Research Council for financial support (GPlates Project).

References

Alvey, A., Gaina, C., Kusznir, N.J., Torsvik, T.H., 2008. Integrated Crustal Thickness Mapping & Plate Reconstructions for the High Arctic. Earth Planet. Sci. 274, 310-321.

Argus, D.F., Gordon, R.G., 1991. No-net-rotation model of current plate velocities incorporating plate motion model NUVEL-1. Geophys. Res. Lett. 18, 2039–2042.

Becker, T.W., 2006. On the effect of temperature and strain-rate dependent viscosity on global mantle flow, net rotation, and plate-driving forces. Geophys. J. Int. 167, 943-957.

Becker, T.W., 2008. Azimuthal seismic anisotropy constrains net rotation of the lithosphere. Geophys. Res. Lett. 35, doi:10.1029/2007GL032928.

Bird, P., 2003. An updated digital model of plate boundaries. Geochem. Geophys. Geosyst. 4, 1027, doi:10.1029/2001GC000252.

Boyden, J.R., Müller, R.D., Gurnis, M., Torsvik, T.H., Clark, J., Turner, M., Ivey-Law, H., Watson, R., Cannon, J., 2010. Next-Generation Plate-Tectonic Reconstructions using GPlates. Geoinformatics, eds. Randy Keller and Chaitan Baru, Cambridge University Press (in press).

Čadek, O., Ricard, Y., 1992. Toroidal/poloidal energy partitioning and global lithospheric rotation during Cenozoic time. Earth Planet. Sci. Lett. 109, 621-632.

Doglioni, C., Green, D.H., Mongelli, F., 2005. On the shallow origin of hotspots and the westward drift of the lithosphere. Geol. Soc. Am. Spec. Paper 388, 735-749.

Duncan, R.A., Clague, D.A., 1985. Pacific plate motion recorded by linear volcanic chains, in The Ocean Basins and Margins, vol.7a, The Pacific Ocean, edited by A. E. M. Nairn, F. G. Stehli, and S. Uyeda, pp. 89–121, Plenum, New York.

Funiciello, F., Facenna, C., Heuret, A., Lallemand, S., Di Giuseppe, E., Becker, T.W., 2008. Trench migration, net rotation and slab-mantle coupling. Earth Planet Sci. Lett. 271, 233-240.

Gaina, C., Roest, W., Müller, R.D., 2002. Late Cretaceous-Cenozoic deformation of northeast Asia. Earth Plan. Sci. Lett. 197, 273-286

Gaina, C., Gernigon, L., Ball, P., 2009. Paleocene-Recent Plate Boundaries in the NE Atlantic and the formation of Jan Mayen microcontinent, J. Geol. Soc. London 166, 601-616.

Gaina, C., Müller, R.D., 2007, Cenozoic tectonic and depth/age evolution of the Indonesian gateway and associated back-arc basins. Earth Sci. Rev. 83, 177-203.

Gaina, C., Müller, R.D., Royer, J.-Y., Stock, J., Hardebeck, J., Symonds, P., 1998, The tectonic history of the Tasman Sea: A puzzle with thirteen pieces. J. Geophys. Res. 103, 12413-12433.

Gripp, A., Gordon, R.G., 2002. Young tracks of hotspots and current plate velocities. Geophys. J. Int. 150, 321-361.

Gordon, R.G., Jurdy, D.M., 1986. Cenozoic global plate motions. J. Geophys. Res. 91, 12 389–12 406.

Gurnis, M., Hall, C., Lavier, L., 2004, Evolving force balance during incipient subduction. Geochem. Geophys. Geosys. *5*, Q07001, doi:10.1029/2003GC00068.

Gurnis, M., Turner, M., DiCaprio, L., Spasojevic, S., Müller, R.D., Boyden, J., Seton, M., Manea, V.C., Bower, D.J., 2010. Global plate reconstructions with continuously closing plates. Geochem. Geophys. Geosys. (in review).

Husson, L., Conrad, C.P., Facenna, C., 2008. Tethyan closure, Andean Orogeny, and westward drift of the Pacific Basin. Earth Planet. Sci. Lett. 271, 303-310.

Heine, C., Müller, R.D, Gaina, C., 2004. Reconstructing the Lost Eastern Tethys Ocean Basin: Convergence history of the SE Asian margin and marine gateways, in *Continent-*

Ocean Interactions in the East Asian Marginal Seas, American Geophysical Union Monograph, pp. 37-54.

Kreemer, C., 2009. Absolute plate motions constrained by shear wave splitting orientations with implications for hot spot motions and mantle flow. J. Geophys. Res. 114, B10405, doi:10.1029/2009JB006416.

Kreemer, C., Holt, W.E., 2001. A no-net-rotation model of present-day surface motions. Geophys. Res. Lett. 28, 4407–4410.

Le Pichon X., 1968. Sea-floor spreading and continental drift. J. Geophys. Res. 73, 3661-97.

Lithgow-Bertelloni, C., Richards, M.A., Ricard, Y., O'Connell, R.J., Engebretson, D.C., 1993. Toroidal-poloidal partitioning of plate motions since 120 Ma. Geophys. Res. Lett. 20, 375-378.

McKenzie, D.P., Parker, R.L., 1967. The North Pacific: An example of tectonics on a sphere. Nature 216, 1276-80.

Morgan, W.J., 1968. Rises, trenches, great faults and crustal blocks. J. Geophys. Res. 73, 1959-1982.

Morgan, W.J., Morgan, J.P., 2007. Plate velocities in the hotspot reference frame. Geol. Soc. Am. Spec. Paper 430, 65-78.

Müller, R.D., Sdrolias, M., Gaina, C., Roest, W., 2008. Age, spreading rates and spreading asymmetry of the world's ocean crust. Geochemistry Geophysics Geosystems, 9, Q04006, doi:10.1029/2007GC001743.

O'Connell, R.J., Gable, C.W., Hager, B.H., 1991. Toroidal-poloidal partitioning of lithospheric plate motions, in Glacial Isostasy, Sea-Level and Mantle Rheology, edited by R. Sabadini, Kluwer Academic Publishers, 535–551.

O'Neill, C., Müller, R.D., Steinberger, B., 2005. On the uncertainties in hot spot reconstructions and the significance of moving hot spot reference frames. Geochem. Geophys. Geosyst. 6, Q04003, doi:10.1029/2004GC000784.

Ricard, Y., Doglioni, C., Sabadini, R., 1991. Differential Rotation Between Lithosphere and Mantle: A Consequence of Lateral Mantle Viscosity Variations. J. Geophys. Res. 96, 8407–8415.

Steinberger, B., Gaina, C., 2007. Plate tectonic reconstructions predict part of Hawaiian hotspot track to be preserved in Bering Sea. Geology 35, 407-410.

Steinberger, B., Torsvik, T.H., 2008. Absolute plate motions and true polar wander in the absence of hotspot tracks. Nature 452, 620-623.

Torsvik, T.H., Tucker, R.F., Ashwal, L.D., Carter, L.M., Jamtveit, B., Vidyadharan, K.T., Venkataramana, P., 2000. Late Cretaceous India-Madagascar fit and timing of break-up related magmatism. Terra Nova 12, 220-224.

Torsvik, T.H., Müller, R.D., Van der Voo, R., Steinberger, B., Gaina, C., 2008a. Global Plate Motion Frames: Toward a unified model. Rev. Geophys. 46, RG3004, doi:10.1029/2007RG000227.

Torsvik, T.H., Gaina, C., Redfield, T.F., 2008b. Antarctica and Global Paleogeography: From Rodinia, through Gondwanaland and Pangea, to the birth of the Southern Ocean and the opening of gateways. In Cooper, A. K., P. J. Barrett, H. Stagg, B. Storey, E. Stump, W. Wise, and the 10th ISAES editorial team (eds.) Antarctica: A Keystone in a Changing World. Proceedings of the 10th International Symposium on Antarctic Earth Sciences. Washington, DC: The National Academies Press, 125-140

Torsvik, T.H., Rousse, S., Labails, C., Smethurst, M.A., 2009. A new scheme for the opening of the South Atlantic Ocean and dissection of an Aptian Salt Basin. Geophys. J. Intern. 177, 1315-1333.

van der Meer, D.G., Spakman, W., van Hinsbergen, D.J.J., Amaru, M.L., Torsvik, T.H., 2010. Towards absolute plate motions constrained by lower-mantle slab remnants. Nature Geoscience, DOI:10.1038/NGEO708.

Wang, S., Wang, R., 2001. Current plate velocities relative to hotspots: implications for hotspot motion, mantle viscosity and global reference frame. Earth Planet. Sci. Lett.. 189, 133-140.

Wilson, J.T., 1966. Did the Atlantic close and then reopen? Nature 211, 676-681.

Table 1 Absolute motions for the African and Pacific plates. African (Plate 701) motions are in an Indo-Atlantic mantle (moving hotspot) frame after 100 Ma (O'Neill et al. 2005) and a TPW corrected palaeomagnetic frame before that (Torsvik et al. 2008a; Steinberger & Torsvik 2008). Pacific (Plate 901) motions are based on a mantle (moving hotspot) frame back to 83 Ma (Steinberger & Gaina, 2008) and then a fixed hotspot frame back to 150 Ma (Duncan & Clague 1985).

	Indo-Atlantic (Africa)			**Pacific**		
Age (Ma)	Lat.(°)	Long.(°)	Angle(°)	Lat.(°)	Long.(°)	Angle(°)
10	46.2	-87.9	-1.9	72.6	-63.7	8.5
20	45.2	-78.6	-4.0	72.6	-63.7	17.0
30	43.5	-69.7	-6.1	71.1	-62.1	23.4
40	44.6	-54.3	-8.1	68.7	-60.1	27.7
50	37.0	-58.9	-10.3	65.0	-63.4	31.4
60	23.7	-42.1	-12.5	57.2	-72.5	34.0
70	20.7	-39.1	-13.8	53.6	-73.8	35.7
80	17.7	-36.1	-15.0	51.1	-74.0	37.3
90	14.6	-33.3	-16.2	49.1	-74.9	41.7
100	14.4	-29.6	-20.1	47.6	-76.0	47.3
110	6.6	330.5	-26.8	51.4	-74.1	50.8
120	6.1	334.9	-30.5	54.7	-72.1	54.5
130	5.9	334.6	-33.8	57.5	-70.1	58.3
140	7.6	334.1	-38.5	60.0	-68.1	62.3
150	10.3	332.3	-37.3	62.2	-66.0	66.4

Table 2 Net rotation calculations.

Time (Ma)	**Net Rotation (°/My)**	**Latitude (°)**	**Longitude (°)**
**5-0*	*0.13*	*-67.5*	*132.1*
*10-0	0.14	-69.3	122.5
*20-10	0.15	-77.0	109.8
*30-20	0.10	-61.5	103.2
40-30	0.10	-14.1	94.2
50-40	0.08	19.5	17.6
60-50	0.33	-6.5	33.7
70-60	0.16	18.9	70.1
80-70	0.18	2.8	114.1
90-80	0.32	-30.3	101.0
100-90	0.28	-10.8	94.9
110-100	0.30	-54.4	-21.8
120-110	0.25	-34.4	63.2
130-120	0.24	-25.6	-12.4
140-130	0.25	-8.7	-5.6
150-140	0.23	-5.8	115.3

*Pronounced Westward drift

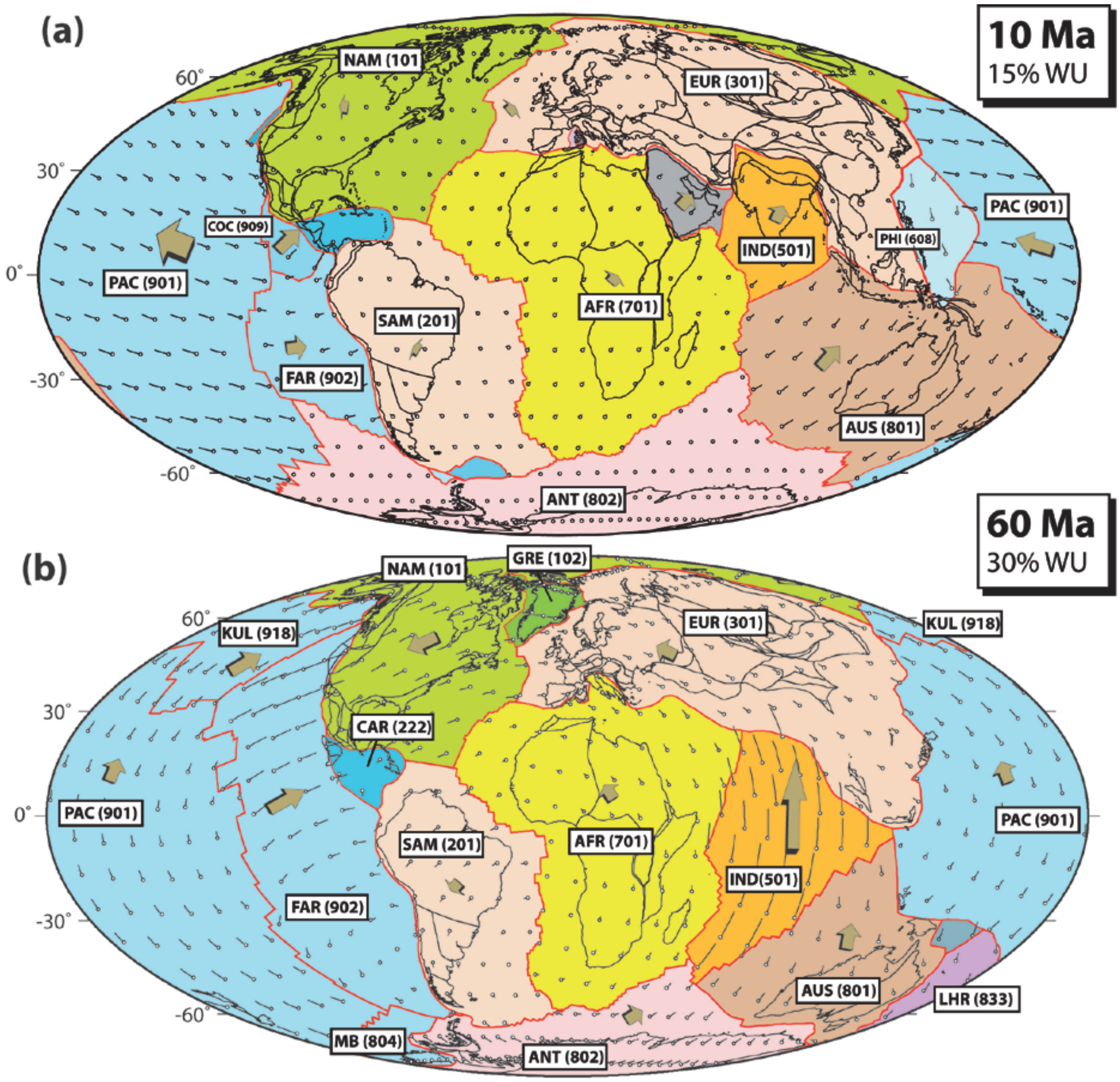

Figure 1 (Torsvik et al.)

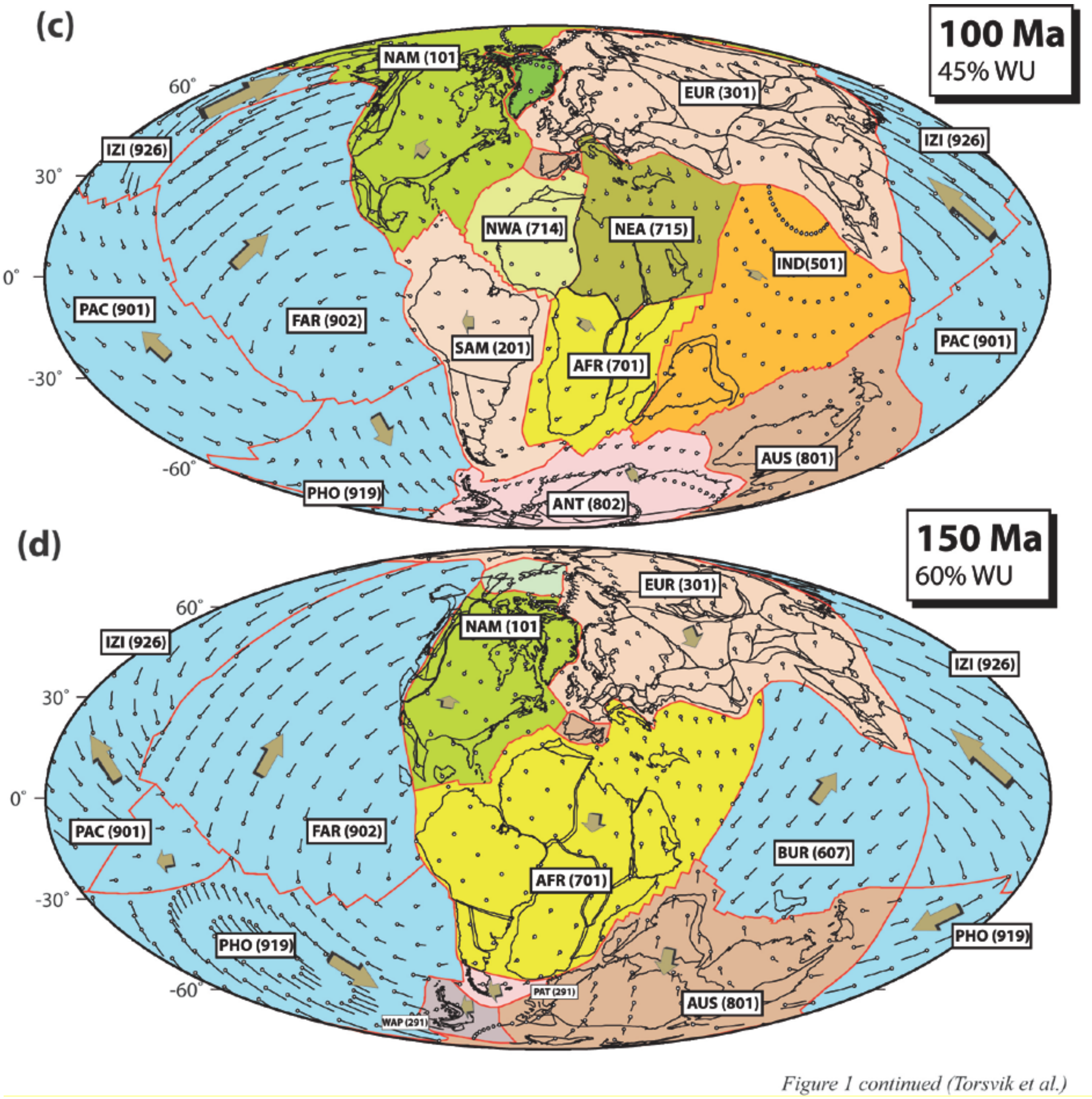

FIGURE 1 Global plate reconstructions and plate polygons (red lines) at 10, 60, 100 and 150 Ma. Dominantly Oceanic plates are shaded blue. Absolute velocity fields are projected 5 My forward from the reconstructed age. Exaggerated (brown) arrows show the generalized velocity pattern. WU=world uncertainty. We also show as black lines the continental part of the plates, mostly present coastlines and intra-plate boundaries that were active at various times through the Phanerozoic. Extended continental margins are not distinguished. NAM=North America, EUR=Europe, IND=India, AFR=South Africa, NWA=Northwest Africa, NEA=Northeast Africa, SAM=South America, PAT=Patagonia, WAT=West Antarctica, MB=Marie Byrdland, AUS=Australia, ANT=East Antarctica, GRE=Greenland, PAC=Pacific, FAR=Farallon, COC=Cocos, PHO=Phoenix, KUL=Kula, CAR=Caribbean, BUR=Burma, PHI=Philippine, LHR=Lord Howe Rise. Mollweide projection.

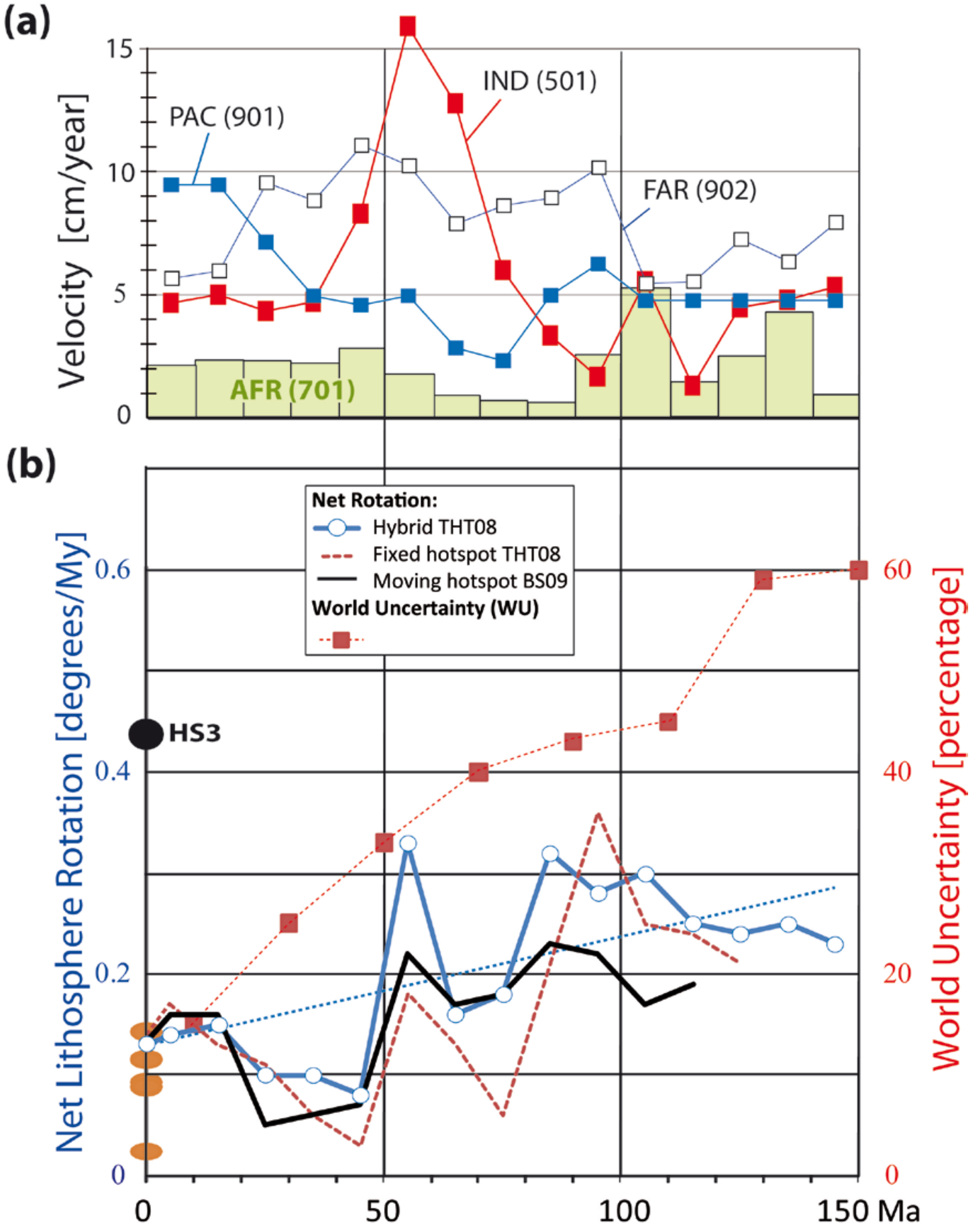

Figure 2 (Torsvik et al.)

FIGURE 2 (a) Absolute point velocity for some selected plates, Africa (AFR: 5°S, 15°E), Pacific (PAC: 0°, 200°E), India (IND:15°N, 75°E) and Farallon (FAR:20°S, 270°E) (b) Net lithosphere rotation (NR) calculated from our plate polygons and reference frames and estimated world uncertainty (WU in %), i.e. essentially the fraction of lithosphere subducted since that time. NR shows fluctuations and a gradual increase with time (see fitted linear trend in stippled blue for the hybrid TPW corrected plate model; Hybrid THT08). The latter we relate to increasing WU ('making up more and more' of oceanic plates). NR for the past 150 Ma probably averages to 0.12°/Ma. For comparison we also show a fixed hotspot model for the last 130 Ma (Torsvik et al. 2008a) and a revised global moving hotspot frame (BS09) based on the New England, Tristan and Reunion hotspots in the African hemisphere (work in progress). Orange ovals are the range of NR values calculated from geodynamic models (Becker 2006, *table 4*). Black circle marked HS3 is the NR value (0.44°/My) calculated from the fixed hot spot model of Gripp & Gordon (2002).

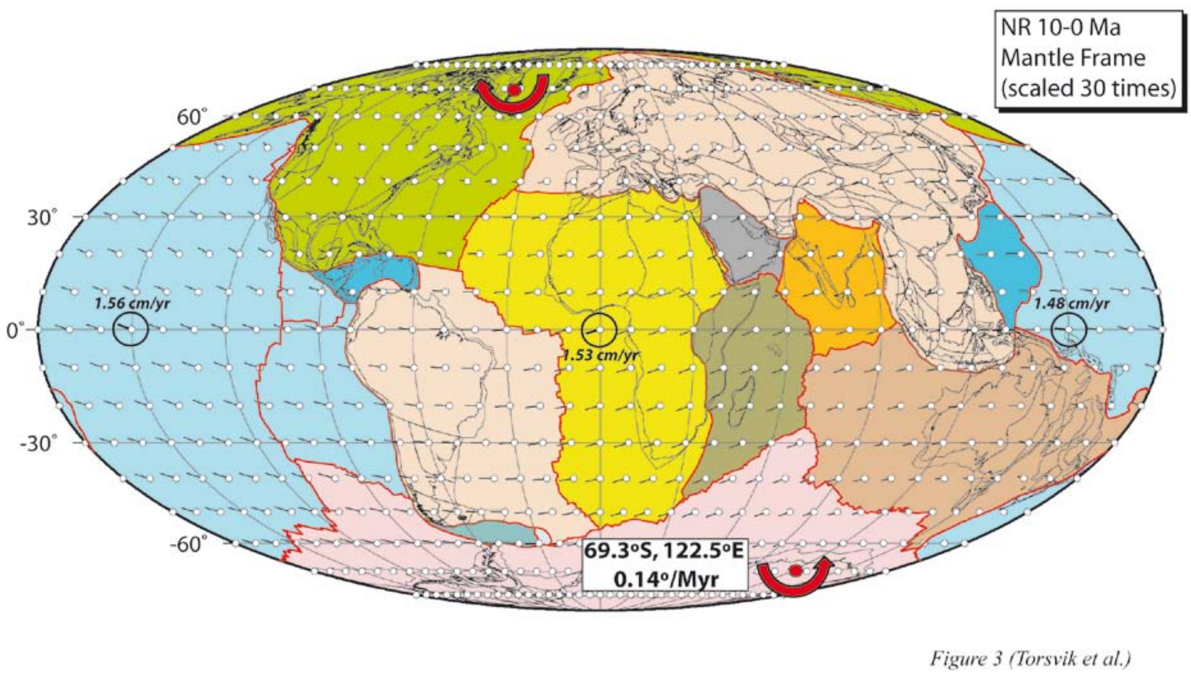

FIGURE 3 Net rotation velocity field (10 x 10° grid) from 10 Ma to present. Because the counterclockwise net rotation pole is at high southerly latitudes (69.3°S, 122.5°E) this results in westward drift. We calculate the total vector velocity at three equatorial locations (1.48-1.56 cm/year; vectors with black circles). The NR velocity field is draped on a simplied present day plate polygon model. Mollweide projection.

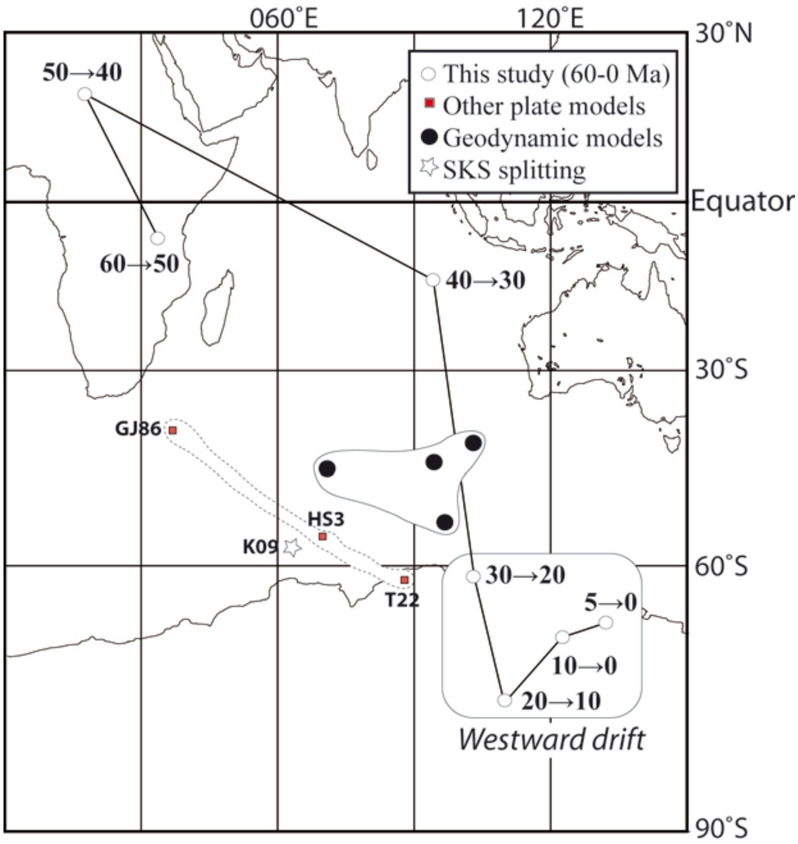

Figure 4 (Torsvik et al.)

FIGURE 4 NR Euler poles for the past 60 My (Table 2) compared with Euler poles from some other plate tectonic (GJ86, Gordon & Jurdy 1986; HS3, Gripp & Gordon 2002; T22, Wang & Wang 2001), and geodynamic models (Becker 2006, *table 4*) and inferred from SKS splitting (K09, Kreemer 2009). From our analysis westward drift is only pronounced for the last 30 Myr. Galls projection.

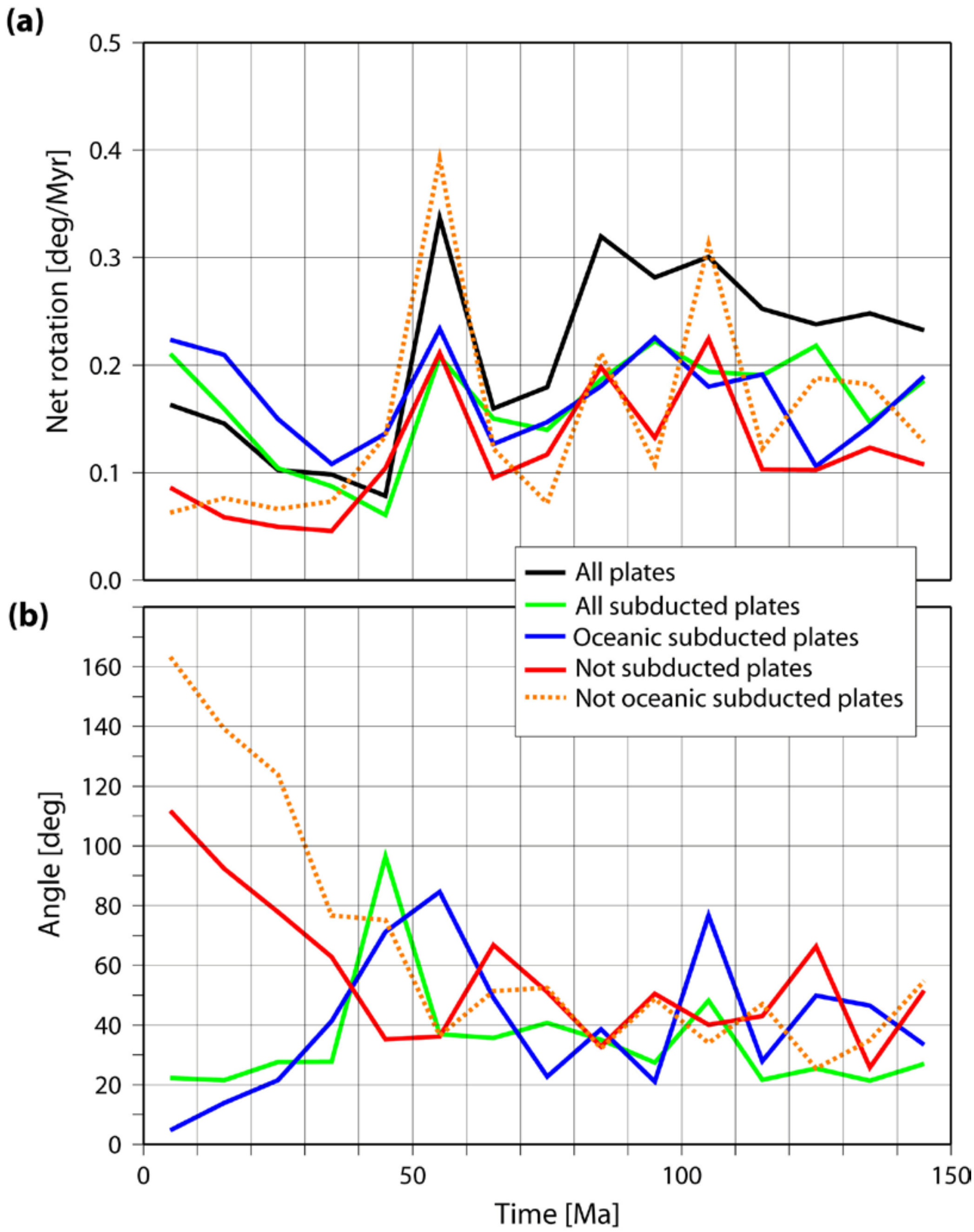

Figure 5 (Torsvik et al.)

FIGURE 5 Net rotations for subsets of plates. (a) NR for all plates (black), for all subducted plates (green), for oceanic subducted plates (blue), for not subducted plates (red; complementary set to green) and for not oceanic subducted plates (stippled orange; complementary to blue). (b) Angle between the axes of net rotation for all plates, and the same subsets of plates as in (a), with same color codes.

Supplementary Materials

Digital reconstructed plate boundaries (0-150 Ma), stage poles (Filename: *0_150_StagePoles.dat*) averaged over 10 Myr (e.g. stage pole at 20 Ma is calculated from 20 to 10 Ma) and a Fortran program (Filename: *bplates.f)* that re-computes the plate boundaries for different absolute rotations than given in Table 1), can be downloaded at http://www.geodynamics.no/poly/PlateTectonics.zip. Stage poles are also listed below (Table S1) followed by a brief description of *bplates.f*. Digital plate boundaries are provided in two different file formats: (1) Standard 'PLATES' ASCHII format (filename: *0_150_Reconstructed.dat*) and (2) Arc-Gis Shape format (three files named: *0_150_Reconstructed.shp, 0_150_Reconstructed.shx, 0_150_Reconstructed.DBF*).

Table S1: Stage Poles

Time	**Latitude**	**Longitude**	**ω (^{o}/Myr)**	**PlateId (Name)**
10	6.08	-37.65	0.48	840 (Aluk)
10	84.00	130.58	0.16	820 (Scotia)
10	51.17	-170.38	0.15	802 (Antarctica)
10	25.31	42.52	0.58	801 (Australia)
10	37.92	-100.31	0.60	902 (Farallon)
10	51.60	14.71	-0.19	201 (Amazonia)
10	3.74	40.01	-0.12	224 (Caribbean)
10	18.20	-107.00	1.97	909 (Cocos)
10	25.42	151.97	-1.25	608 (Philippine Sea)
10	51.31	-11.74	0.42	503 (Arabia)
10	40.39	14.55	0.50	501 (India)
10	46.19	-87.86	0.19	701 (South Africa)
10	17.70	13.98	-1.32	322 (Calabria)
10	38.76	-140.30	0.16	306 (Corsica-Sardinia)
10	20.25	-81.77	-0.25	903 (Juan de Fuca)
10	72.61	-63.73	-0.85	901 (Pacific)
10	38.76	-140.30	0.16	301 (Europe)
10	36.90	76.50	-0.19	101 (North America)
20	4.66	-37.93	0.56	840 (Aluk)
20	32.47	-8.05	-0.13	820 (Scotia)
20	62.10	-117.82	0.13	802 (Antarctica)
20	11.12	-127.40	-0.34	847 (Solomon)
20	77.57	170.91	0.57	902 (Farallon)
20	20.21	171.41	-0.92	688 (SW Caroline Basin)
20	28.04	24.46	0.58	801 (Australia)
20	52.77	1.76	-0.25	201 (Amazonia)
20	21.56	23.96	-0.15	224 (Caribbean)

20	29.29	-127.45	1.73	909 (Cocos)
20	12.99	154.53	-1.66	608 (Philippine Sea)
20	12.28	155.44	-2.02	659 (Izu-Bonin-Mariana)
20	45.34	-21.58	0.45	501 (India)
20	54.96	-10.93	0.55	322 (Calabria)
20	54.96	-10.93	0.55	306 (Corsica-Sardinia)
20	43.52	-70.47	0.21	701 (South Africa)
20	3.59	103.85	0.24	903 (Juan de Fuca)
20	72.61	-63.73	-0.85	901 (Pacific)
20	44.62	-118.57	0.16	301 (Europe)
20	41.20	88.34	-0.22	101 (North America)
30	15.70	-33.95	0.23	840 (Aluk)
30	56.85	152.08	0.12	804 (Marie Byrdland)
30	40.10	22.82	1.27	838 (NW South Fiji Basin)
30	69.32	144.73	0.10	802 (Antarctica)
30	53.60	48.94	1.04	839 (East South Fiji Basin)
30	33.12	16.83	1.11	847 (Solomon)
30	6.21	134.97	-1.59	688 (SW Caroline Basin)
30	3.56	132.70	-1.35	689 (NE Caroline Basin)
30	9.68	143.96	-1.35	690 (SE Caroline Basin)
30	9.68	143.96	-1.35	653 (NW Caroline Sea)
30	21.95	33.76	0.64	801 (Australia)
30	56.20	-1.61	-0.26	201 (Amazonia)
30	10.36	155.74	-1.90	659 (Izu-Bonin-Mariana)
30	30.64	22.56	-0.15	224 (Caribbean)
30	16.22	150.34	-0.82	608 (Philippine Sea)
30	64.06	-175.95	0.88	902 (Farallon)
30	19.79	33.31	0.66	501 (India)
30	38.13	-54.99	0.21	701 (South Africa)
30	62.65	175.87	1.00	903 (Juan de Fuca)
30	67.26	-56.76	-0.64	901 (Pacific)
30	15.52	-126.82	0.11	301 (Europe)
30	47.38	80.37	-0.21	101 (North America)
40	9.32	-27.44	0.29	840 (Aluk)
40	32.44	136.46	0.20	804 (Marie Byrdland)
40	39.94	113.14	0.12	802 (Antarctica)
40	25.76	37.35	0.54	857 (North Loyalty Basin)
40	43.41	4.59	2.23	847 (Solomon)
40	25.76	37.35	0.54	801 (Australia)
40	4.52	121.25	1.14	645 (Celebes Sea)
40	13.07	-24.77	-0.08	608 (Philippine Sea)
40	6.95	165.29	0.53	665 (North Celebes)
40	72.95	-47.88	-0.25	201 (Amazonia)
40	5.47	-67.48	-0.28	222 (Caribbean)
40	35.56	29.69	0.59	501 (India)

40	16.65	-73.96	-0.55	609 (North Philippine Sea)
40	36.32	-18.16	0.24	701 (South Africa)
40	58.73	129.45	1.00	902 (Farallon)
40	56.75	-48.47	-0.45	901 (Pacific)
40	56.75	-48.47	-0.45	918 (Kula)
40	50.16	97.69	-0.13	102 (Greenland)
40	13.07	-24.77	-0.08	301 (Europe)
40	84.31	104.90	-0.22	101 (North America)
50	35.53	-151.09	0.16	804 (Marie Byrdland)
50	35.96	-137.44	0.14	802 (Antarctica)
50	45.79	-22.46	0.10	801 (Australia)
50	38.42	-64.62	-0.42	901 (Pacific)
50	55.45	56.18	-0.35	201 (Amazonia)
50	32.22	70.29	-0.28	224 (Caribbean)
50	17.75	-12.78	0.77	501 (India)
50	12.17	-71.76	0.26	701 (South Africa)
50	55.97	121.05	1.35	902 (Farallon)
50	32.39	-59.93	-0.92	918 (Kula)
50	26.37	83.44	-0.39	102 (Greenland)
50	20.23	53.48	-0.24	301 (Europe)
50	52.81	85.54	-0.38	101 (North America)
60	5.84	-165.16	-0.43	804 (Marie Byrdland)
60	23.80	-172.19	-0.47	802 (Antarctica)
60	40.57	-129.25	-0.66	833 (Lord Howe Rise)
60	39.38	-93.66	-0.90	836 (Louisiade Plateau)
60	21.23	-169.22	-0.57	801 (Australia)
60	48.38	169.11	-0.62	201 (Amazonia)
60	6.11	-59.57	1.56	222 (Caribbean)
60	0.01	177.76	-1.59	501 (India)
60	17.59	167.05	-0.45	701 (South Africa)
60	1.31	100.29	0.56	901 (Pacific)
60	46.17	108.69	1.41	902 (Farallon)
60	14.93	127.89	1.25	918 (Kula)
60	47.96	144.88	-0.60	102 (Greenland)
60	54.12	165.01	-0.40	301 (Europe)
60	41.78	161.63	-0.69	101 (North America)
70	78.51	96.70	0.18	802 (Antarctica)
70	31.33	-53.09	-0.67	833 (Lord Howe Rise)
70	59.60	49.68	0.18	801 (Australia)
70	79.30	159.06	-0.29	201 (Amazonia)
70	17.78	-2.87	1.21	501 (India)
70	4.29	-69.10	-0.28	901 (Pacific)
70	8.46	161.04	-0.16	701 (South Africa)
70	40.02	-107.58	-1.46	926 (Izanagi)
70	54.22	138.14	0.87	902 (Farallon)

70	10.24	135.76	-0.11	102 (Greenland)
70	74.69	-2.60	-0.16	301 (Europe)
70	79.97	145.36	-0.34	101 (North America)
80	18.98	122.89	0.56	833 (Lord Howe Rise)
80	11.27	147.93	0.27	802 (Antarctica)
80	9.00	133.29	0.24	801 (Australia)
80	73.01	-24.38	-0.51	201 (Amazonia)
80	18.89	10.44	0.60	501 (India)
80	7.98	-62.33	-0.22	901 (Pacific)
80	14.16	165.01	-0.16	701 (South Africa)
80	55.90	151.69	0.90	902 (Farallon)
80	40.36	-110.10	-1.41	926 (Izanagi)
80	71.11	45.51	-0.17	102 (Greenland)
80	78.71	56.90	-0.16	301 (Europe)
80	74.18	-2.72	-0.51	101 (North America)
90	22.29	-48.45	-0.52	802 (Antarctica)
90	20.12	143.88	-0.56	919 (Phoenix)
90	28.85	-56.60	-0.53	801 (Australia)
90	32.34	-73.60	-0.46	901 (Pacific)
90	52.26	-23.09	-0.56	201 (Amazonia)
90	22.51	-138.87	-1.37	501 (India)
90	60.63	6.99	-0.48	305 (Armorica)
90	19.26	168.58	-0.17	701 (South Africa)
90	43.50	120.32	0.97	902 (Farallon)
90	40.48	-107.44	-1.68	926 (Izanagi)
90	62.55	9.32	-0.43	102 (Greenland)
90	60.63	6.99	-0.48	301 (Europe)
90	65.86	0.00	-0.64	101 (North America)
100	69.11	123.42	0.29	802 (Antarctica)
100	9.51	-165.25	-0.75	919 (Phoenix)
100	20.05	87.66	0.16	801 (Australia)
100	10.58	-15.40	0.40	701 (South Africa)
100	61.65	-27.27	-0.34	201 (Amazonia)
100	35.99	-76.01	-0.58	901 (Pacific)
100	28.00	-14.81	0.15	501 (India)
100	10.58	-15.40	0.40	714 (NW Africa)
100	54.40	26.35	-0.38	305 (Armorica)
100	12.23	-16.40	0.41	715 (NE Africa)
100	37.85	115.74	1.08	902 (Farallon)
100	38.97	-106.44	-1.80	926 (Izanagi)
100	60.06	31.12	-0.36	102 (Greenland)
100	54.40	26.35	-0.38	301 (Europe)
100	63.75	24.02	-0.43	101 (North America)
110	37.13	-119.42	0.19	802 (Antarctica)
110	14.41	145.81	-0.74	702 (Madagascar)

110	14.47	165.98	-0.93	919 (Phoenix)
110	84.89	-26.89	-0.30	801 (Australia)
110	14.41	145.81	-0.74	701 (South Africa)
110	64.22	101.08	-0.61	201 (Amazonia)
110	85.01	165.04	-0.48	901 (Pacific)
110	20.87	135.52	-0.51	501 (India)
110	14.41	145.81	-0.74	714 (NW Africa)
110	46.91	95.92	-0.76	304 (Iberia)
110	13.11	145.65	-0.75	715 (NE Africa)
110	52.71	135.03	0.64	902 (Farallon)
110	50.26	102.63	-0.84	102 (Greenland)
110	49.77	-119.16	-1.63	926 (Izanagi)
110	47.38	101.78	-0.81	301 (Europe)
110	53.48	101.13	-0.87	101 (North America)
120	34.54	128.47	0.46	802 (Antarctica)
120	4.84	-178.65	-0.43	702 (Madagascar)
120	17.24	-68.75	-0.50	801 (Australia)
120	14.50	170.65	-0.93	919 (Phoenix)
120	4.84	-178.65	-0.43	701 (South Africa)
120	44.62	-160.55	-0.25	201 (Amazonia)
120	85.01	165.03	-0.48	901 (Pacific)
120	9.40	-157.00	-0.19	501 (India)
120	4.84	-178.65	-0.43	714 (NW Africa)
120	23.47	7.22	2.50	304 (Iberia)
120	2.80	-179.59	-0.44	715 (NE Africa)
120	67.47	76.47	-0.47	102 (Greenland)
120	52.52	139.33	0.64	902 (Farallon)
120	50.18	-114.48	-1.63	926 (Izanagi)
120	64.20	82.98	-0.43	301 (Europe)
120	70.06	69.71	-0.52	101 (North America)
130	72.20	100.92	0.86	803 (Antarctic Peninsula)
130	13.16	-99.12	-0.20	802 (Antarctica)
130	1.93	-138.97	0.21	291 (Patagonia)
130	31.22	-126.66	-0.23	702 (Madagascar)
130	16.41	-128.58	0.18	202 (Parana)
130	1.93	-138.97	0.21	290 (Colorado)
130	7.17	116.11	-1.72	919 (Phoenix)
130	17.06	-99.74	-0.21	801 (Australia)
130	4.70	-28.38	0.33	701 (South Africa)
130	0.10	-83.75	0.22	201 (Amazonia)
130	85.01	165.03	-0.48	901 (Pacific)
130	0.00	114.82	-0.28	714 (NW Africa)
130	29.58	-161.07	-0.97	501 (India)
130	30.38	75.27	-0.46	304 (Iberia)
130	4.84	-28.39	0.33	715 (NE Africa)

130	22.65	96.90	0.68	902 (Farallon)
130	43.00	-115.80	-1.43	926 (Izanagi)
130	8.60	87.25	-0.48	103 (Arctic Alaska)
130	31.01	77.59	-0.47	101 (North America)
130	31.01	77.59	-0.47	301 (Europe)
140	42.68	143.20	-1.07	803 (Antarctic Peninsula)
140	24.65	-33.11	0.33	291 (Patagonia)
140	28.09	-28.27	0.40	202 (Parana)
140	26.36	-30.83	0.36	290 (Colorado)
140	23.84	37.45	0.21	801 (Australia)
140	12.82	121.54	-1.35	919 (Phoenix)
140	12.48	-1.40	0.46	501 (India)
140	85.01	165.03	-0.48	901 (Pacific)
140	20.45	-29.04	0.47	201 (Amazonia)
140	2.26	129.85	-0.41	304 (Iberia)
140	19.71	-25.62	0.49	701 (South Africa)
140	12.97	-25.79	1.40	607 (Burma-Enderby)
140	3.87	129.99	-0.43	101 (North America)
140	20.45	144.13	0.58	902 (Farallon)
140	48.53	-98.98	-1.30	926 (Izanagi)
140	42.29	-46.70	1.32	103 (Arctic Alaska)
140	3.87	129.99	-0.43	301 (Europe)
150	67.59	145.77	-0.75	803 (Antarctic Peninsula)
150	35.30	172.69	0.25	291 (Patagonia)
150	10.46	122.08	0.51	801 (Australia)
150	17.24	125.57	-0.93	919 (Phoenix)
150	85.01	165.03	-0.48	901 (Pacific)
150	0.37	10.16	-0.39	304 (Iberia)
150	47.65	171.27	0.25	701 (South Africa)
150	37.37	-18.56	1.01	607 (Burma-Enderby)
150	3.82	12.46	-0.38	101 (North America)
150	19.38	154.50	0.73	902 (Farallon)
150	66.14	-56.97	2.02	103 (Arctic Alaska)
150	46.93	-97.59	-1.58	926 (Izanagi)
150	2.38	12.51	-0.38	301 (Europe)

Description of *bplates.f*

We supply a routine *bplates.f* that modifies plate boundaries consistent with a change of Africa and Pacific absolute plate rotations, while relative rotations within the Pacific and African hemispheres remain the same. The sample input file *bplates.in* specifies in the first seven lines:

1. the number of finite rotations per plate
2. the file with the new Pacific plate rotations, for which the new set of plate boundaries is created. Rotations need to be given the same way as in Table 1 (age, latitude, longitude, angle), and ages need to correspond to the input plate boundary file. However, the first rotation needs to correspond to the first set of boundaries with *non-zero* ages - boundaries for zero age are left unmodified. Therefore the rotation file should not contain a first line with zeroes, even though the plate boundary file contains the set of present-day boundaries. If the number of time intervals before present for which plate boundaries are given is larger than the number of rotations, then boundaries for time intervals before the oldest rotation are not rotated.
3. the file with the new Africa rotations.
4. the file with the original Pacific rotations (Table 1) used to generate the existing set of plate boundaries.
5. the file with the original Africa rotations (Table 1).
6. The existing file with plate boundaries *0_150_Reconstructed.dat* which is also provided in this online supplement.
7. The output file for the modified plate boundaries (given as closed polygons around each plate; one file for all time intervals, like the input file)

The remaining lines contain the names of four output files per time interval: First (here "….d1") for all boundaries in that time interval, then "...d2" for boundaries between two "African set" plates, "...d3" between two "Pacific set" plates and "...d4" between one "African set" and one "Pacific set" plate. For each boundary between two plates, the "header" contains the number of points, the ID numbers of plates on the "left" and "right" side of the boundary, and secondary plate ID numbers assigned consecutively at each time interval: in case plates have the same primary ID number in the same time interval, the secondary number is always unique.

In brief, the program *bplates.f* performs the following steps:

- In a "pre-processing", closed polygons around each plate are split up into individual boundaries between two plates.
- These boundaries are rotated according to the change from "old" to "new" rotations (program lines 146-168): Plates are separated into "African" and "Pacific" sets. The

"Pacific" set includes all plates with ID # >900. Back to 80 Ma (i<=80) no Phoenix plate exists in our model, and the “Pacific” set additionally includes plates 802 (Antarctica), 804 (Bellinghausen/Marie Birdland) and 840 (Aluk). In the interval 0-10 Ma, it also includes plate 820 (Scotia). Boundaries within the Pacific set are rotated according to Pacific rotations. Boundaries between the Pacific and African sets or within the African set of plates are rotated according to African rotations. This step disconnects plate boundaries within the Pacific set of plates from the "ring" separating the Pacific and African sets.

- All points of boundaries within the Pacific set, that end up on the African set of plates after the rotations, are removed, in order to avoid boundaries crossing each other.
- Remaining boundaries within the Pacific set are connected to the closest points on the "ring" surrounding the Pacific set.
- The "post-processing" re-combines rotated and re-connected boundaries to closed polygons.